Nanoscale Horizons

ROYAL SOCIETY OF CHEMISTRY

COMMUNICATION

View Article Online
View Journal | View Issue

Open Access Article. Published on 30 July 2025. Downloaded on 11/8/2025 9:24:44 PM.
This article is licensed under a Creative Commons Attribution 3.0 Unported Licence.

Check for updates

Cite this: *Nanoscale Horiz.*, 2025, **10**, 2945

Received 15th May 2025,
Accepted 28th July 2025

DOI: 10.1039/d5nh00347d

rsc.li/nanoscale-horizons

Influence of anchoring group on charge transport across self-assembled monolayer-based molecular tunnel junctions

Qianqian Guo,[a] Shi Huang,[a] Xiaojiang Yu,[b] Christian A. Nijhuis *[c] and Xiaoping Chen *[ad]

Predicting the charge transport rate, mechanism and dielectric response of solid-state molecular electronics is challenging since these properties depend on many variables such as molecular backbone, electrode material, junction contact geometry, anchoring and terminal functional groups, and so on. Although the effects of the anchoring group (X) on the conductance of single-molecule junctions have been widely investigated, in large-area junctions examples are rare, although the latter makes it possible to also explore the role of dielectric properties on charge transport rates. Here we report a change of 2.5 orders of magnitude in the charge transport rate along with a factor of 3 change in the measured dielectric constant (ε_r) across monolayers of $X(C_6H_4)_nH$ with n = 1 or 2 and X = NO_2, SH, NH_2, CN, and Pyr. Our combined study involving current–voltage measurements and impedance spectroscopy allowed us to isolate the contact (R_C) and monolayer resistance (R_{SAM}), and found that the R_C increased with the X order. This change in R_C goes hand-in-hand with the shift of HOMO and LUMO energy levels with respect to the Fermi levels of the electrodes explaining the large observed change in charge transport rate. Surprisingly, the increase in tunneling rates (or decrease in R_{SAM}) scales with ε_r. Our work provides new insights into the factors that influence the charge transport rate and dielectric response of molecular junctions besides widely studied changes to the molecular backbone or terminal functional groups.

[a] *Fujian Provincial Key Laboratory of Modern Analytical Science and Separation Technology, Fujian Provincial Key Laboratory of Pollution Monitoring and Control, College of Chemistry, Chemical Engineering and Environment, Minnan Normal University, Zhangzhou 363000, China. E-mail: xiaopingchen@mnnu.edu.cn*

[b] *Singapore Synchrotron Light Source, National University of Singapore, 5 Research Link, Singapore 117603, Singapore*

[c] *Hybrid Materials for Opto-Electronics Group, Department of Molecules and Materials, MESA+ Institute for Nanotechnology and Molecules Centre, Faculty of Science and Technology, University of Twente, 7500 AE Enschede, The Netherlands. E-mail: c.a.nijhuis@utwente.nl*

[d] *Centre for Advanced 2D Materials and Graphene Research Centre, National University of Singapore, 6 Science Drive 2, Singapore 117546, Singapore*

New concepts

Molecular junctions, in the form of metal–molecule–metal, have been found to be important in a large range of areas including catalysis, energy generation and storage, sensing, and nano-electronics. A long-standing open question is "how do molecules conduct charge carriers at the smallest possible length scales where quantum effects dominate?". The conductivity and the dielectric response of molecular junctions depend on many variables such as molecular backbone, electrode material, anchoring and terminal functional groups, *etc.* Although the role of the impact of molecular backbone, electrode or terminal functional groups on junction conductance have been widely studied, the role of the anchoring groups is rarely studied in large area junctions. To fill this gap, we conducted current density and impedance characterizations for junctions with monolayers of different anchoring groups. We found the change in anchoring group resulted in large differences in the conductivity and dielectric constant of the junctions. The change in anchoring group induced differences in the dielectric response and the shifts of HOMO and LUMO levels with respect to the Fermi levels of the electrodes explaining the observed changes in conductivity. Our work provides new insights into the factors that influence the charge transport rates and dielectric response of molecular junctions.

Introduction

Understanding and precisely controlling the charge transport rate across molecules attached to interfaces is important in a large range of areas including catalysis,[1] energy storages,[2,3] sensing,[4] nano-electronics,[5,6] and artificial intelligence,[7] for example. Solid-state molecular junctions make it possible to obtain detailed new insights into the charge transport mechanisms of molecular diodes,[8–10] switches,[11] memristors[12–15] or transistors,[16,17] or to study thermoelectric,[18,19] spintronic,[20] or plasmonic[21] effects at the molecular length scales. In principle, by designing the molecular structure of the junctions the, desired charge transport rate and electronic function can be achieved. So far, this envisioned predictive molecular control has been challenging to achieve because molecules interact with the electrodes and form a new physical-organic system whose properties depend on several intertwined parameters.

Open Access Article. Published on 30 July 2025. Downloaded on 11/8/2025 9:24:44 PM.
This article is licensed under a Creative Commons Attribution 3.0 Unported Licence.

In large-area junctions (normally in the form of M–XB$_n$T//M, here M = metal electrode, X = anchoring group, B = backbone, n = number of repeating unit, T = terminal group, "–" represents a covalent bond, and "//" indicates a physical contact interface), systematic studies of structural changes of self-assembled monolayer (SAM) on charge transport tend to be focused on T which forms a physical contact with the top electrode[22–24] or changes to B.[5,25–27] The effects of X on charge transport rate are largely unexplored[28–31] (although in single-molecule junctions the role of X has been studied in more detail[32–37]). In addition, the role of dielectric response on charge transport rate is still rarely explored in molecular junctions despite initial theoretical and experimental studies demonstrating its important role.[22,38–40] Here, we show that the X of Au–X(C$_6$H$_4$)$_n$H//GaO$_x$/EGaIn (n = 1 or 2 and X = –NO$_2$, –SH, –NH$_2$, –CN, and –Pyr, EGaIn represents eutectic alloy of gallium and indium) junctions changes the charge transport rate by 2.5 orders of magnitude and the ε_r by a factor of 3 (from 1.2 to 3.5). This work reinforces earlier observations where molecules in junctions have surprising large ε_r leading to a large increase in the tunnelling rate.[22,39]

The charge transport rate, the mechanism of charge transport, and the value of ε_r of molecular junctions are determined by many factors, *i.e.*, the type of X,[32,35,37,41,42] B,[43] T,[22–24] or the type of electrode,[44,45] which all affect the tunneling barrier height (ΔE), the molecule–electrode coupling strength (Γ), and therefore the associated potential profile across the junctions. In molecular junctions, both the molecule–electrode interfaces have to be considered. By introducing T to monolayers, one can influence the monolayer—top-electrode interface. Depending on the nature of T, the monolayer—top electrode interface can be, *e.g.*, covalent,[44,45] van der Waals[8,9,22,38] or ionic[46] in nature. Similarly, by changing X where X can be thiol (–SH), nitrite (–NO$_2$), sulfonate (–SO$_3^-$), hydroxyl (–OH), nitrile (–CN), amine (–NH$_2$), carboxylic acid (–COOH), benzyl (–C$_6$H$_6$), and pyridyl (–C$_6$H$_5$N), the nature of the monolayer—bottom-electrode interactions can be changed.[47,48] By changing X, however, the binding geometry (including tilt angle, orientation or packing) may vary but also the electronic structure of the junctions.[32,49,50] For X = SH, the formation of a S–Au bond can result in a highest occupied molecular orbital (HOMO) level localized at the S–Au, supporting HOMO mediated charge transport.[45,51] In contrast, the X = NO$_2$, CN, or Pyr interacts with the electrode *via* the O and N atoms, respectively, resulting in a lowest unoccupied molecular orbital (LUMO) dominated conduction.[32,44,52] Therefore, differences in X can lead to variations in conductance and rectification behaviour of junctions.[31,53,54]

The conductance of single molecule junctions with different X of the general form of M–XB$_n$X–M has been widely investigated, but there is no consensus on the effects of X on conductance.[32–37] For example, for conjugated backbones, Borguet's group reported conductance of single-porphyrin junctions of Au–X(porphyrin)X–Au with different X following the sequence of Pyr > NH$_2$ > –SO$_3^-$ > CN > COOH, and the Pyr exhibited higher conductance than others due to a strong binding interaction of the N–Au bond.[33] In contrast, Wandlowski's group found that the conductance of junctions of functionalized oligoynes (Au–X(C$_6$H$_4$)C≡C(C$_6$H$_4$)C≡C(C$_6$H$_4$)X–Au) and tolanes (Au–X(C$_6$H$_4$)C≡C(C$_6$H$_4$)X–Au) followed the sequence of bisthiol > SH > NH$_2$ > Pyr > CN,[34,55] which agreed with Ratner and coworkers' computational results.[56,57] In the case of X = NO$_2$, Erbe and coworkers found junctions of Au–X(C$_6$H$_4$)C≡C(C$_6$H$_4$)X–Au with a conductance sequence of NO$_2$ > SH > CN where for X = NO$_2$ the conductance was ∼17 times larger than for X = CN.[32] For junctions with saturated molecular backbones the behavior is different. Tao and coworkers found for Au–X(CH$_2$)$_n$X–Au junctions that the binding strength follows the sequence of SH > NH$_2$ > COOH but the conductance follows the sequence of SH > COOH > NH$_2$.[36]

In contrast, in large area SAM-based molecular junctions the role of X is rarely investigated.[28–31] Frisbie and coworkers found the change of X in Au–X(phenyl)$_n$//Au junctions from NC to SH affected the resistance of SAM by almost one order due to the change in HOMO with respect to the Fermi level of the electrode (E_F) but the β values were close to each other.[30] Whitesides and coworkers found that junctions of M–X(C$_6$H$_4$)$_n$//GaO$_x$/EGaIn (X = SH and HC ≡ C) showed similar values of β and contact resistance, while the X = HSCH$_2$ series decoupled the phenyl ring from SH and confined the HOMO orbital onto the S atom, resulting in an increase in β.[29] Cahen and colleagues could largely tune the Si(111)–(CH$_2$)$_2$(C$_6$H$_4$)X//Hg junctions from Ohmic behaviour to strong rectifiers and the associated potential profiles by changing X from Br to CH$_3$ or H.[58] Recently, Li and colleagues extended the X from SH to diselenide and achieved extremely stable junctions for over 200 days.[28]

In principle, strong dipoles at the metal–molecule interfaces or molecular dipoles could lead to changes in energy level alignment and electrostatic potential profile of the junction thereby changing the measured tunneling rates,[23,41,57] but usually those effects are relatively small leading to changes in measured current of no more than one order of magnitude.[26,59] Recently we found that molecular polarizability can have large effects on the charge transport rates[22,38,60] and even lead to changes in the mechanism of charge transport.[8,25,27,38] The role of polarizability can be investigated by measuring the dielectric constant ε_r *via* capacitance measurements (but the capacitance of single-molecule junctions is too small to be measurable).[39,61] For example, the tunnelling rate changed by 4 orders of magnitude along with a 4-fold increase in ε_r in large area junctions of Ag–S(CH$_2$)$_n$T//GaO$_x$/EGaIn (T = F, Cl, Br, or I) by only changing the polarizability of T.[22] In contrast, changing permanent dipoles in large area junctions with the same electrodes did not change the tunneling rates significantly across a broad range of different types of T.[23,24,62,63] For aromatic junctions in the form of Au–S(C$_6$H$_4$)$_n$T//GaO$_x$/EGaIn, the polarizability of T had no significant effect on the measured tunneling rates or ε_r for T = F, Cl, Br or I due to collective electrostatic effects. These collective effects arise from induced opposite electric fields in neighbouring molecules resulting in small effective dipoles and are important to consider in conjugated, densely packed SAMs.[23,63] These strong collective electrostatic effects in Au–S(C$_6$H$_4$)$_n$T//GaO$_x$/EGaIn junctions lead to confinement of the electrostatic potential at the

Open Access Article. Published on 30 July 2025. Downloaded on 11/8/2025 9:24:44 PM.
This article is licensed under a Creative Commons Attribution 3.0 Unported Licence.

terminal position T and to similar effective tunnelling barrier heights regardless of T.

For all of these reasons, it is important to measure both changes in current and ε_r in charge transport studies across large area junctions. Here, we applied soft EGaIn as the top electrode and SAMs of X(C$_6$H$_4$)$_n$H to study the influence of X on the charge transport rate and ε_r of Au–X(C$_6$H$_4$)$_n$H//GaO$_x$/EGaIn junctions. The current changes by 2.5 orders of magnitude and ε_r by a factor of 3 in a descending order of X = –NO$_2$, –SH, –NH$_2$, –CN, and –Pyr. The shifts in HOMO and LUMO with respect of the E_F of the electrodes, and the changes in ε_r and Γ induced by X are responsible for the large change in the measured charge transport rates. Our work deepens the understanding of the charge transport mechanisms across molecular electronic devices and shows that changes in X can have profound effects on their electronic and dielectric properties.

Results and discussion

Fig. 1a shows the schematic illustration of the Au–X(C$_6$H$_4$)$_n$H//GaO$_x$/EGaIn junction consisting of a SAM on Au (Au–SAM) with a conjugated backbone and different X. Using large-area junctions, we were not only able to derive the effects of X on charge transport rate, but also to determine the contributions of the resistance of SAM (R_{SAM}, in Ω cm^2), the contact resistance of the junction (R_C, in mΩ cm^2), the capacitance of SAM (C_{SAM}, in μF cm^{-2}) and the ε_r of SAM from impedance spectroscopy.[39,61] Fig. 1b shows the shift of HOMO, LUMO, and the associated ΔE defined by the HOMO (ΔE_{HOMO}) or LUMO (ΔE_{LUMO}), which is the energy offset between the HOMO or LUMO and E_F of the electrodes. The Γ between the X and Au electrode is indicated by the broadening of the molecular levels. With the possible changes in ΔE and Γ as a function of X, we anticipated to measure differences in charge transport rate and ε_r.

Surface characterization of the SAMs on Au

To study the structure and packing quality of the Au–SAM, we formed the SAMs on template-stripped Au and characterized these SAMs using angle-resolved X-ray photoelectron spectroscopy (ARXPS) and ultraviolet photoelectron spectroscopy (UPS; see Section S3). The C 1s in Fig. S2 and N 1s in Fig. S3 show the presence of NO$_2$, NH$_2$, CN, and Pyr, respectively. The S 2p spectra (Fig. S4a and b) are dominated by doublet peaks with the characteristic S 2p$_{3/2}$ signal at 161.8 eV, indicating the metal–thiolate bond formation.[63] The O 1*s* spectrum for X = NO$_2$ shows a single peak at 532.5 eV (Fig. S4c and d) which corresponds to the NO$_2$ interacting with the metal surface.[64,65] From ARXPS at two emission angles θ of 40° and 90°, we calculated the thickness ($d_{SAM,XPS}$, in Å) and surface coverage of SAM ($\Psi_{SAM,XPS}$, in 10^{-10} mol cm^{-2}). Fig. 2a shows that the $d_{SAM,XPS}$ for all investigated SAMs is within error (the instrumental and fitting error of 10%) the same and in good agreement with the molecular length calculated from the space-filling model (L_{CPK}, Table 1). Fig. 2b shows that the relative surface coverage of SAMs to S(C$_6$H$_4$)$_2$ of 7.69 × 10^{-10} mol cm^{-2} is also within error the same. From these XPS measurements we also derived the tilt angle α (in °) with respect to the surface normal (Table 1) from which we conclude that all SAMs have similar up-right structure with comparable packing densities in agreement with previous reports.[63,64,66]

Fig. S6 shows the UPS spectra from which we derived the work function of Au modified with SAM, Φ_{SAM} (in eV), and the ΔE_{HOMO} values (in eV) from the secondary electron cut-off and the valence band, respectively. Fig. 2c shows that the Φ_{SAM} values are essentially independent of X and close to 4.4 eV likely due to Fermi-level pinning.[30,45,57] The optical HOMO–LUMO gaps of the different molecules were characterized using UV-vis spectroscopy (Fig. S7 and Table 1). The optical HOMO–LUMO gap varies from 3.51 eV of X = NO$_2$ to 4.31 eV of X = Pyr. Based on these data, we constructed the energy level diagrams (Fig. 1b) with the HOMO pinned and with varying values of E_{LUMO} (Table 1) calculated from the energy difference between E_{HOMO} and the optical HOMO–LUMO gap, and ΔE_{LUMO} was calculated from the difference between E_{LUMO} and Φ_{SAM}.

J(*V*) characterization of molecular junctions

We recorded current density–voltage ($J(V)$, J in A cm^{-2} and V in V) curves for the various molecular junctions using cone-shaped tips of EGaIn as described previously.[9,67] For each type of junction, we recorded ∼400 $J(V)$ curves from ∼20 junctions and subsequently computed the Gaussian logarithmic mean of

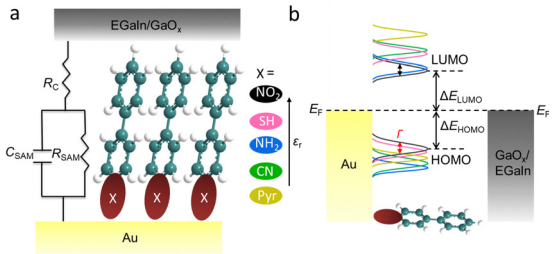

Fig. 1 (a) Schematic illustration of the Au–X(C$_6$H$_4$)$_n$H//GaO$_x$/EGaIn junction with n = 1 or 2 and X = –NO$_2$, –SH, –NH$_2$, –CN, and –Pyr where "–" indicates covalent bond, "//" indicates the non-covalent contact and "/" represents the physical phase between GaO$_x$ and EGaIn. In all experiments, the bottom gold electrode was grounded, while the voltage was applied to the top EGaIn electrode. (b) The proposed energy level alignment of the SAMs embedded in Au and GaO$_x$/EGaIn leads was based on our experimental results. The coupling strength between molecule and electrode Γ (schematically indicated by changes in the width given by the double arrow in red), ΔE_{HOMO}, and ΔE_{LUMO} (given by the double arrows in black) of the SAMs in the junction vary with X.

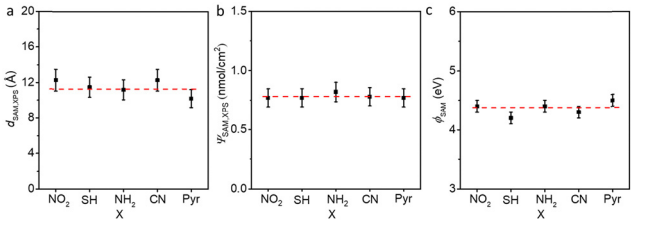

Fig. 2 (a) $d_{SAM,XPS}$ and (b) $\Psi_{SAM,XPS}$ of the SAMs on Au obtained from ARXPS. (c) Φ_{SAM} *vs.* X obtained from UPS. The error bars represent the instrumental and fitting error of 10%. The red dashed lines are visual guides.

Open Access Article. Published on 30 July 2025. Downloaded on 11/8/2025 9:24:44 PM.
This article is licensed under a Creative Commons Attribution 3.0 Unported Licence.

Table 1 Summary of the spectroscopy data of Au–X(C_6H_4)$_n$H SAMs

X	$d_{SAM,XPS}$ (Å)[a]	$\Psi_{SAM,XPS}$[a] ($\times 10^{-10}$ mol cm^{-2})	L_{CPK}	α (°)[b]	E_{HOMO} (eV)[c]	ΔE_{HOMO} (eV)[c]	Φ_{SAM} (eV)[c]	Optical gap (eV)	E_{LUMO} (eV)[d]	ΔE_{LUMO} (eV)[d]
NO_2	12.3	7.66	12.8	16.1	−6.2	1.8	−4.4	3.51	−2.69	1.71
SH	11.5	7.69	12.5	23.1	−6.1	1.9	−4.2	4.05	−2.05	2.15
NH_2	11.2	8.17	12.2	23.3	−6.5	2.1	−4.4	3.84	−2.66	1.74
CN	12.3	7.84	13.4	23.4	−6.3	2.0	−4.3	4.11	−2.19	2.11
Pyr	10.2	7.70	10.8	19.2	−6.3	1.8	−4.5	4.31	−1.99	2.51

[a] ARXPS was used to calculate $d_{SAM,XPS}$ and relative $\Psi_{SAM,XPS}$ (relative to Ψ_{SAM} of S(C_6H_4)$_2$ SAM on Au of 7.69×10^{-10} mol cm^{-2}).[66] Errors for both $d_{SAM,XPS}$ and $\Psi_{SAM,XPS}$ represent instrumental and fitting errors of 10%. [b] The tilt angle was calculated from the molecular length from CPK model and $d_{SAM,XPS}$. [c] UPS was used to obtain E_{HOMO}, ΔE_{HOMO} and Φ_{SAM}. The error represents the resolution of UPS which is ±0.1 eV. [d] The E_{LUMO} was calculated from the E_{HOMO} + optical gap, the ΔE_{LUMO} was calculated from $E_{LUMO} - \Phi_{SAM}$.

$|J|$, $\langle \log_{10}|J| \rangle_G$, as well as the Gaussian logarithmic standard deviation, $\sigma_{log,G}$ (see Fig. S8 and Table S1). Fig. 3a shows $\langle \log_{10}|J| \rangle_G$ *vs.* V for Au–X(C_6H_4)$_n$H//GaO_x/EGaIn junctions at V = ±0.5 V. Fig. 3b shows the trend of $\langle \log_{10}|J| \rangle_G$ as a function of X at −0.5 V. The data indicate a continuous decrease in $\langle \log_{10}|J| \rangle_G$ from −1.5 ± 0.4 to −4.0 ± 0.4 A cm^{-2} as X changes from NO_2 to Pyr. These findings are different from previous studies on junctions of Au–S(C_6H_4)$_2$T//GaO_x/EGaIn[63] and Au–SC_6H_4T//GaO_x/EGaIn[23] which also had aromatic backbones where a change in T along the series of halides (F, Cl, Br and I) had negligible influence on the charge transport rate and ε_r due to collective electrostatic effects (also found in other types of conjugated junctions[68–70]). However, the evolution of $\langle \log_{10}|J| \rangle_G$ *vs.* X generally follows the conductance measured in single-molecule junctions by Erbe,[32] Wandlowski,[34,55] and Tao,[36] and theoretical calculations from Ratner[56,57] which could be explained with changes in Γ and associated shift of relevant molecular frontier orbitals. These findings indicate that collective electrostatic effects play a role for terminal functionalization at the top of the SAM, but apparently do not cancel contributions of X. Data from single-molecule junctions, such as Au–X(porphyrin)X–Au, showed that X = Pyr exhibited higher conductance than X = CN since the Γ of N–Au bond is stronger.[33] In contrast, we found that X = Pyr has the lowest charge transport rate. Molecules with X = Pyr also have the largest optical HOMO–LUMO gap of 4.31 eV and associated ΔE_{LUMO} of 2.51 eV in our study which could be the reason for the low conductivity. The increase of $\langle \log_{10}|J| \rangle_G$ from X = NO_2 to X = Pyr is 2.5 orders of magnitude while from the simplified Simmons' equation of $J = J_0 e^{-\beta d^{SAM}}$ where $\beta \propto \sqrt{\Delta E_{LUMO}}$, J_0 is the pre-exponential factor, β is the tunneling decay coefficient (in Å^{-1}),[22,39] it can be estimated that the difference in ΔE of 0.8 eV (see Table 1 for ΔE_{LUMO} values) can roughly account for only one order of magnitude difference in current. The difference in Γ and the dielectric properties of the junctions could contribute to the further change in charge transport rate.

According to prior works, SH bonded molecules have a HOMO level close to E_F of the gold bottom electrode.[45,47,57,63] The junctions with X = SH have a small ΔE_{HOMO} of 1.9 eV (Fig. 4a and Table 1) and therefore the charge transport mechanism most likely proceeds by hole transport *via* the HOMO explaining why X = SH does not follow the trend in Fig. 4c. In contrast, for junctions with X of –NO_2, –NH_2, –CN, and –Pyr, the charge transport mechanism is expected to be mediated by the LUMO. From Fig. 4b and c, the optical gap of the SAMs generally increases in the sequence of NO_2, NH_2, CN, to Pyr, which results in an increase of ΔE_{LUMO} and the decrease of current across the junctions, explaining the current trend plotted in Fig. 3b. All these observations also explain the lack of a clear trend in Fig. 4a. Fig. 4 also shows that the ΔE_{LUMO} of 1.7 eV for X = NO_2 is smaller than the ΔE_{HOMO} of 1.9 eV for X = SH explaining (at least in part) why the former results in higher tunneling rates than the latter.

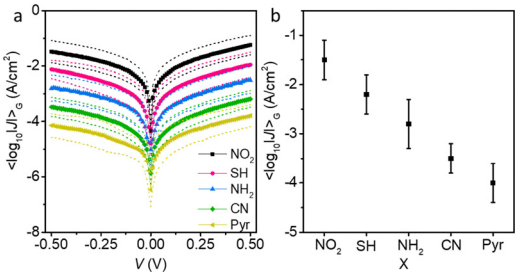

Fig. 3 (a) Curves of $\langle \log_{10}|J| \rangle_G$ *vs.* V of Au–X(C_6H_4)$_n$H//GaO_x/EGaIn junctions. (b) $\langle \log_{10}|J| \rangle_G$ *vs.* X for all the junctions. The dashed lines in Panel a and error bars in Panel b indicate the Gaussian logarithmic standard deviation, $\sigma_{log,G}$.

Impedance characterization of molecular junctions

The current response across molecular junctions to the DC bias applied is an overall response to all the resistances coming from the circuit. Impedance spectroscopy is a powerful technique to separate the R_{SAM}, R_C, and C_{SAM}.[39,61] Fig. 1a shows the equivalent circuit to which our data was fitted. As reported

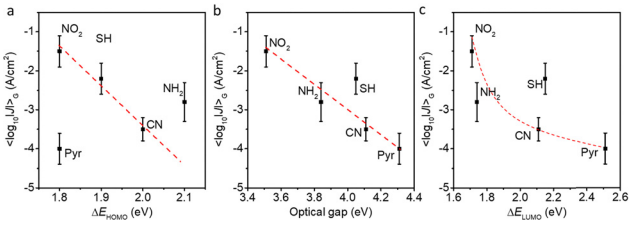

Fig. 4 $\langle \log_{10}|J| \rangle_G$ *vs.* ΔE_{HOMO} (a), optical HOMO–LUMO gap (b), and ΔE_{LUMO} (c) for Au–X(C_6H_4)$_n$H//GaO_x/EGaIn junctions with X indicated in the plots. The error bars indicate $\sigma_{log,G}$. The red dashed lines are visual guides.

Open Access Article. Published on 30 July 2025. Downloaded on 11/8/2025 9:24:44 PM.
This article is licensed under a Creative Commons Attribution 3.0 Unported Licence.

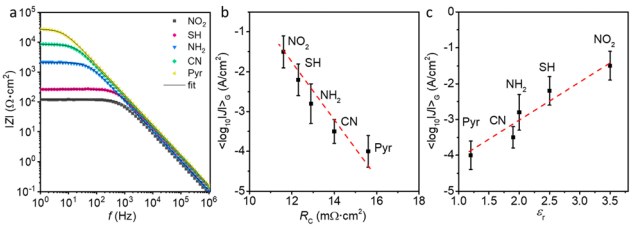

Fig. 5 Bode plots (a), $\langle \log_{10}|J|\rangle_G$ *vs.* R_C (b) and ε_r (c) for different types of junctions. The errors of $\langle \log_{10}|J|\rangle_G$ come from $\sigma_{\log,G}$. The red dashed lines are visual guides.

before, this circuit contains a R_C in series with a parallel combination of R_{SAM} and C_{SAM}.[39,61] As described previously, we employed EGaIn top electrodes which were confined in the microchannels of polydimethylsiloxane (PDMS) to form the top electrical contacts to SAMs.[22,39,61] The impedance spectra were recorded using a 30 mV amplitude sinusoidal voltage at a DC bias of 0 V, across a frequency range from 1 Hz to 1 MHz with 10 points per decade. The acquired raw data were fitted to the equivalent circuit (Fig. 1a) to derive the R_{SAM}, R_C, C_{SAM} and ε_r (calculated from C_{SAM} by eqn (S3)) values. The fitted Bode, Nyquist, and phase plots are shown in Fig. S9. When X changes from NO_2 to Pyr, the complex impedance $|Z|$ (Fig. 5a) and the value of R_{SAM} (Table S2) change by more than two orders of magnitude with R_{SAM} increasing from $(1.6 \pm 0.9) \times 10^2\ \Omega\ cm^2$ to $(2.5 \pm 0.7) \times 10^4\ \Omega\ cm^2$, which agrees well with the trend of $\langle \log_{10}|J|\rangle_G$. Moreover, the values of R_C (Fig. 5b) changes from $11.6 \pm 1.6\ m\Omega\ cm^2$ for X = NO_2 to $15.6 \pm 1.9\ m\Omega\ cm^2$ for X = Pyr. This change is small but significant, given that we usually assume that R_C is dominated by the SAM//GaO_x/EGaIn van der Waals interface where also the GaO_x layer contributes to R_C.[61] Since for all SAMs the SAM//GaO_x/EGaIn interface was not changed, the change in R_C reflects the changes in the X and associated changes in the Au–SAM interface. The change in R_C indicates a change in Γ at the SAM–Au interface which results in a larger transmission probability according to the Landauer's formulism.[22] Since $R_C \ll R_{SAM}$, changes in R_C alone cannot account for the large change in current densities shown in Fig. 3.

From the measured values of C_{SAM}, the ε_r values of the junctions can be derived (using the parallel plate capacitor equation; Table S2). We note that the presence of water can increase the measured value of ε_r in the case if hydrophilic oligoglycine and oligoglycol SAMs.[38] Due to the hydrophobic nature of the SAMs used in the present study, we believe that water does not play a significant role. Fig. 5c shows that $\langle \log_{10}|J|\rangle_G$ increases with ε_r from X = Pyr ($\varepsilon_r = 1.2 \pm 0.3$) to X = NO_2 ($\varepsilon_r = 3.5 \pm 0.1$). This observation agrees with our earlier findings that in general the measured tunneling rates increase with increasing dielectric response of molecular junctions. For example, in junctions of Ag–$S(CH_2)_{14}T$//GaO_x/EGaIn, the measured currents increased by 3 orders of magnitude along with a factor 4 times increase in ε_r for F → I.[22] In contrast, when conjugated backbones were applied in the junctions with SAMs of SC_6H_4T,[23] $S(C_6H_4)_2T$,[63] and $S(CH_2)_{10}OPhT_y$,[8] the substituent of T had negligible effects on both the charge transport rate[23,63] and dielectric responses[8,23,63] due to the collective electrostatic effects of the phenyl rings.[68] In contrast, for non-conjugated SAMs T can have large effects.[22]

Here, the charge transport rate and dielectric response are both affected by X despite the collective electrostatic effects from the aromatic backbone.

Conclusions

In this work, we employed SAMs with conjugated backbones and different X of $X(C_6H_4)_2H$ to investigate the effects of X on energy level alignment, charge transport rates, and dielectric response of EGaIn-based molecular junctions. Previous studies reported that collective electrostatic effects induced by the conjugated backbones compensate the effects of dipoles or polarizable groups,[23,63,68] but here we show that a change in X results in a significant increase in charge transport rate of 2.5 orders of magnitude along with a 3 fold increase in ε_r. Furthermore, depending on the X, the charge transport mechanism changes between HOMO or LUMO mediated tunneling. Although the X did change the tunneling barrier height ΔE defined by the HOMO or LUMO by ~0.8 eV, this change cannot quantitively explain the observed changes in tunneling rate (or measured current). For similar reasons, the small change in the contact resistance R_C can also not explain the large changes in measured current. The dielectric properties, however, play an important role in charge transport rate because it directly relates to the shape of the electrostatic potential profile. Since in our experiments we only changed the X, our results imply that an increase in ε_r will mostly affect the potential drop at the bottom electrode–SAM interface which in turn enhances the transmission probability.[22,60] A possible explanation why different polar moieties at the Au–SAM interface lead to much larger effects than for similar junctions but with the polar groups placed at the SAM//GaO_x/EGaIn interface could be due to the covalent nature of the Au–SAM interface and that the electrostatic potential profile extends deeper into the SAM than for physiosorbed SAM//GaO_x/EGaIn interfaces.[22] It would be interesting to study these effects for different bottom-electrode materials (such as Ag or Pt). Our work shows that anchoring groups can have a profound effect on the charge transport properties of large-area junctions providing an alternative for optimizing electronic properties and that it is important to consider the dielectric properties of molecular junctions in attempts to quantitatively model tunneling rates.

Author contributions

X. C., Q. G., and S. H. characterised and analysed the compounds electrically. X. C., Q. G., and X. Y. characterised and analysed the XPS and UPS. Q. G. conducted the optical measurements. X. C. and C. A. N. conceptualised and led the study. All the authors discussed the data and wrote the manuscript together.

Open Access Article. Published on 30 July 2025. Downloaded on 11/8/2025 9:24:44 PM.
This article is licensed under a Creative Commons Attribution 3.0 Unported Licence.

Conflicts of interest

There are no conflicts to declare.

Data availability

Data for this article, including $J(V)$ results, UV-vis, XPS, and UPS, impedance are available at **https://dataverse.harvard.edu/dataset.xhtml?persistentId=doi:10.7910/DVN/5I0ME8**.

The data supporting this article have been included as part of the Supplementary information. Supplementary information available: Supplementary information includes materials and instruments; preparation of SAMs; surface XPS and UPS characterization of SAMs on Au; UV-vis optical characterization; electrical $J(V)$ and impedance characterization of molecular junctions. See DOI: **https://doi.org/10.1039/d5nh00347d**

Acknowledgements

X. Chen is thankful for the support under the Eagle Project of Fujian Province, the National Natural Science Foundation of China (Grant No. 22404074), and the President's Fund of Minnan Normal University (Grant No. KJ2023002). C. Nijhuis acknowledges the Dutch Research Council (NWO), VI.C.222.037.

References

1 C. D. Bostick, S. Mukhopadhyay, I. Pecht, M. Sheves, D. Cahen and D. Lederman, Protein bioelectronics: a review of what we do and do not know, *Rep. Prog. Phys.*, 2018, **81**(2), 026601.
2 H. Chen, C. Jia, X. Zhu, C. Yang, X. Guo and J. F. Stoddart, Reactions in single-molecule junctions, *Nat. Rev. Mater.*, 2023, **8**(3), 165–185.
3 X. He, M. Kwon, J. Chung, K. Lee, Y. Choi, Y. Im, J. Jang, Y. Choi and H. J. Yoon, Self-assembled molecular layers as interfacial engineering nanomaterials in rechargeable battery applications, *Small*, 2024, **20**(44), 2403537.
4 M. Courté, A. Hoff, G. C. Welch and L. G. Kaake, Organic heterojunction charge-transfer chemical sensors, *J. Mater. Chem. C*, 2024, **12**(14), 5083–5087.
5 J. Jang and H. J. Yoon, Long-range charge transport in molecular wires, *J. Am. Chem. Soc.*, 2024, **146**(47), 32206–32221.
6 C. Gao, W. Si, Y. Huo, Y. Xiang, G. Li, J. Wang, C. Jia and X. Guo, Device engineering of monolayer-based electronics, *Nano Today*, 2024, **59**, 102472.
7 C. Yan, C. Fang, J. Gan, J. Wang, X. Zhao, X. Wang, J. Li, Y. Zhang, H. Liu, X. Li, J. Bai, J. Liu and W. Hong, From molecular electronics to molecular intelligence, *ACS Nano*, 2024, **18**(42), 28531–28556.
8 X. Chen, I. Volkova, Y. Wang, Z. Zhang and C. A. Nijhuis, Gradual change between coherent and incoherent tunneling regimes induced by polarizable halide substituents in molecular tunnel junctions, *J. Am. Chem. Soc.*, 2024, **146**(33), 23356–23364.
9 X. Chen, M. Roemer, L. Yuan, W. Du, D. Thompson, E. Del Barco and C. A. Nijhuis, Molecular diodes with rectification ratios exceeding 10(5) driven by electrostatic interactions, *Nat. Nanotechnol.*, 2017, **12**(8), 797–803.
10 M. Roemer, X. Chen, Y. Li, L. Wang, X. Yu, P.-A. Cazade, C. Nickle, R. Akter, E. Del Barco, D. Thompson and C. A. Nijhuis, Supramolecular tunnelling junctions with robust high rectification based on assembly effects, *Nanoscale*, 2024, **16**(42), 19683–19691.
11 C. Jia, A. Migliore, N. Xin, S. Huang, J. Wang, Q. Yang, S. Wang, H. Chen, D. Wang, B. Feng, Z. Liu, G. Zhang, D.-H. Qu, H. Tian, M. A. Ratner, H. Q. Xu, A. Nitzan and X. Guo, Covalently bonded single-molecule junctions with stable and reversible photoswitched conductivity, *Science*, 2016, **352**(6292), 1443–1445.
12 Y. Han, C. Nickle, Z. Zhang, H. Astier, T. J. Duffin, D. Qi, Z. Wang, E. Del Barco, D. Thompson and C. A. Nijhuis, Electric-field-driven dual-functional molecular switches in tunnel junctions, *Nat. Mater.*, 2020, **19**(8), 843–848.
13 Z. Wang, Z. Li, C. Li, X. Ji, X. Song, X. Yu, L. Wang and W. Hu, Generic dynamic molecular devices by quantitative non-steady-state proton/water-coupled electron transport kinetics, *Proc. Natl. Acad. Sci. U. S. A.*, 2023, **120**(24), e2304506120.
14 Y. Wang, Q. Zhang, H. Astier, C. Nickle, S. Soni, F. A. Alami, A. Borrini, Z. Zhang, C. Honnigfort, B. Braunschweig, A. Leoncini, D. C. Qi, Y. Han, E. Del Barco, D. Thompson and C. A. Nijhuis, Dynamic molecular switches with hysteretic negative differential conductance emulating synaptic behaviour, *Nat. Mater.*, 2022, **21**(12), 1403–1411.
15 Y. Zhang, L. Liu, B. Tu, B. Cui, J. Guo, X. Zhao, J. Wang and Y. Yan, An artificial synapse based on molecular junctions, *Nat. Commun.*, 2023, **14**(1), 247.
16 Z. Chen, I. M. Grace, S. L. Woltering, L. Chen, A. Gee, J. Baugh, G. A. D. Briggs, L. Bogani, J. A. Mol, C. J. Lambert, H. L. Anderson and J. O. Thomas, Quantum interference enhances the performance of single-molecule transistors, *Nat. Nanotechnol.*, 2024, **19**(7), 986–992.
17 X. Li, Y. Zheng, Y. Zhou, Z. Zhu, J. Wu, W. Ge, Y. Zhang, Y. Ye, L. Chen, J. Shi, J. Liu, J. Bai, Z. Liu and W. Hong, Supramolecular transistors with quantum interference effect, *J. Am. Chem. Soc.*, 2023, **145**(39), 21679–21686.
18 P. He, J. Jang, H. Kang and H. J. Yoon, Thermoelectricity in molecular tunnel junctions, *Chem. Rev.*, 2025, **125**(5), 2953–3004.
19 J. Jang, P. He and H. J. Yoon, Molecular thermoelectricity in EGaIn-based molecular junctions, *Acc. Chem. Res.*, 2023, **56**(12), 1613–1622.
20 X. Gu, L. Guo, Y. Qin, T. Yang, K. Meng, S. Hu and X. Sun, Challenges and prospects of molecular spintronics, *Precis. Chem.*, 2024, **2**(1), 1–13.
21 M. Wang, T. Wang, O. S. Ojambati, T. J. Duffin, K. Kang, T. Lee, E. Scheer, D. Xiang and C. A. Nijhuis, Plasmonic phenomena in molecular junctions: principles and applications, *Nat. Rev. Chem.*, 2022, **6**(10), 681–704.
22 X. Chen, B. Kretz, F. Adoah, C. Nickle, X. Chi, X. Yu, E. del Barco, D. Thompson, D. A. Egger and C. A. Nijhuis, A single

 This journal is © The Royal Society of Chemistry 2025

Open Access Article. Published on 30 July 2025. Downloaded on 11/8/2025 9:24:44 PM.
This article is licensed under a Creative Commons Attribution 3.0 Unported Licence.

atom change turns insulating saturated wires into molecular conductors, *Nat. Commun.*, 2021, **12**(1), 3432.

23 G. D. Kong, M. Kim, H.-J. Jang, K.-C. Liao and H. J. Yoon, Influence of halogen substitutions on rates of charge tunneling across SAM-based large-area junctions, *Phys. Chem. Chem. Phys.*, 2015, **17**(21), 13804–13807.

24 M. Baghbanzadeh, P. F. Pieters, L. Yuan, D. Collison and G. M. Whitesides, The rate of charge tunneling in EGaIn junctions is not sensitive to halogen substituents at the self-assembled monolayer//Ga_2O_3 interface, *ACS Nano*, 2018, **12**(10), 10221–10230.

25 M. Baghbanzadeh, L. Belding, L. Yuan, J. Park, M. H. Al-Sayah, C. M. Bowers and G. M. Whitesides, Dipole-induced rectification across Ag^{TS}/SAM//Ga_2O_3/EGaIn junctions, *J. Am. Chem. Soc.*, 2019, **141**(22), 8969–8980.

26 J. Chen, S. Gathiaka, Z. Wang and M. Thuo, Role of molecular dipoles in charge transport across large area molecular junctions delineated using isomorphic self-assembled monolayers, *J. Phys. Chem. C*, 2017, **121**(43), 23931–23938.

27 A. Kovalchuk, D. A. Egger, T. Abu-Husein, E. Zojer, A. Terfort and R. C. Chiechi, Dipole-induced asymmetric conduction in tunneling junctions comprising self-assembled monolayers, *RSC Adv.*, 2016, **6**(73), 69479–69483.

28 N. Chen, S. Li, P. Zhao, R. Liu, Y. Xie, J.-L. Lin, C. A. Nijhuis, B. Xu, L. Zhang, H. Xu and Y. Li, Extreme long-lifetime self-assembled monolayer for air-stable molecular junctions, *Sci. Adv.*, 2023, **9**(42), eadh3412.

29 C. M. Bowers, D. Rappoport, M. Baghbanzadeh, F. C. Simeone, K.-C. Liao, S. N. Semenov, T. Żaba, P. Cyganik, A. Aspuru-Guzik and G. M. Whitesides, Tunneling across SAMs containing oligophenyl groups, *J. Phys. Chem. C*, 2016, **120**(21), 11331–11337.

30 B. Kim, J. M. Beebe, Y. Jun, X. Y. Zhu and C. D. Frisbie, Correlation between HOMO alignment and contact resistance in molecular junctions: aromatic thiols versus aromatic isocyanides, *J. Am. Chem. Soc.*, 2006, **128**(15), 4970–4971.

31 Q. V. Nguyen, P. Martin, D. Frath, M. L. Della Rocca, F. Lafolet, C. Barraud, P. Lafarge, V. Mukundan, D. James, R. L. McCreery and J. C. Lacroix, Control of rectification in molecular junctions: contact effects and molecular signature, *J. Am. Chem. Soc.*, 2017, **139**(34), 11913–11922.

32 L. A. Zotti, T. Kirchner, J.-C. Cuevas, F. Pauly, T. Huhn, E. Scheer and A. Erbe, Revealing the role of anchoring groups in the electrical conduction through single-molecule junctions, *Small*, 2010, **6**(14), 1529–1535.

33 Z. Li, M. Smeu, M. A. Ratner and E. Borguet, Effect of anchoring groups on single molecule charge transport through porphyrins, *J. Phys. Chem. C*, 2013, **117**(29), 14890–14898.

34 W. Hong, D. Z. Manrique, P. Moreno-García, M. Gulcur, A. Mishchenko, C. J. Lambert, M. R. Bryce and T. Wandlowski, Single molecular conductance of tolanes: experimental and theoretical study on the junction evolution dependent on the anchoring group, *J. Am. Chem. Soc.*, 2012, **134**(4), 2292–2304.

35 S. Li, Y. Jiang, Y. Wang, D. Lin, H. Pan, Y. Wang, S. Sanvito and S. Hou, Oxazine: an anchoring group serving as functional kernels to construct single-molecule switches, *J. Mater. Chem. C*, 2024, **12**(6), 2194–2202.

36 F. Chen, X. Li, J. Hihath, Z. Huang and N. Tao, Effect of anchoring groups on single-molecule conductance: comparative study of thiol-, amine-, and carboxylic-acid-terminated molecules, *J. Am. Chem. Soc.*, 2006, **128**(49), 15874–15881.

37 A. Daaoub, J. M. F. Morris, V. A. Béland, P. Demay-Drouhard, A. Hussein, S. J. Higgins, H. Sadeghi, R. J. Nichols, A. Vezzoli, T. Baumgartner and S. Sangtarash, Not so innocent after all: interfacial chemistry determines charge-transport efficiency in single-molecule junctions, *Angew. Chem., Int. Ed.*, 2023, **62**(24), e202302150.

38 X. Chen, T. Salim, Z. Zhang, X. Yu, I. Volkova and C. A. Nijhuis, Large increase in the dielectric constant and partial loss of coherence increases tunneling rates across molecular wires, *ACS Appl. Mater. Interfaces*, 2020, **12**(40), 45111–45121.

39 X. Chen and C. A. Nijhuis, The unusual dielectric response of large area molecular tunnel junctions probed with impedance spectroscopy, *Adv. Electron. Mater.*, 2022, **8**(2), 2100495.

40 Y. A. Berlin and M. A. Ratner, Conduction of metal-thin organic film-metal junctions at low bias, *J. Phys. Chem. C*, 2018, **122**(13), 7557–7563.

41 V. Obersteiner, D. A. Egger and E. Zojer, Impact of anchoring groups on ballistic transport: single molecule vs monolayer junctions, *J. Phys. Chem. C*, 2015, **119**(36), 21198–21208.

42 D. M. Cegiełka, K. Kozieł, M. Zharnikov and P. Cyganik, Anchoring groups for ordered and highly stable monomolecular films on naturally oxidized aluminum – phosphonate versus carboxylate, *Appl. Surf. Sci.*, 2024, **665**, 160199.

43 H. J. Lee, S. J. Cho, H. Kang, X. He and H. J. Yoon, Achieving ultralow, zero, and inverted tunneling attenuation coefficients in molecular wires with extended conjugation, *Small*, 2021, **17**(12), 2005711.

44 C. E. Smith, Z. Xie, I. Bâldea and C. D. Frisbie, Work function and temperature dependence of electron tunneling through an N-type perylene diimide molecular junction with isocyanide surface linkers, *Nanoscale*, 2018, **10**(3), 964–975.

45 Z. Xie, I. Bâldea, C. E. Smith, Y. Wu and C. D. Frisbie, Experimental and theoretical analysis of nanotransport in oligophenylene dithiol junctions as a function of molecular length and contact work function, *ACS Nano*, 2015, **9**(8), 8022–8036.

46 L. Tian, A. Fan, X. Yu and W. Hu, Achieving high-performance molecular rectification through fast screening alkanethiol carboxylate-metal complexes electroactive units, *CCS Chem.*, 2023, **5**(4), 902–914.

47 L. Sun, Y. A. Diaz-Fernandez, T. A. Gschneidtner, F. Westerlund, S. Lara-Avila and K. Moth-Poulsen, Single-molecule electronics: from chemical design to functional devices, *Chem. Soc. Rev.*, 2014, **43**(21), 7378–7411.

48 V. Kaliginedi, A. V. Rudnev, P. Moreno-García, M. Baghernejad, C. Huang, W. Hong and T. Wandlowski, Promising anchoring groups for single-molecule conductance

Open Access Article. Published on 30 July 2025. Downloaded on 11/8/2025 9:24:44 PM.
This article is licensed under a Creative Commons Attribution 3.0 Unported Licence.

measurements, *Phys. Chem. Chem. Phys.*, 2014, **16**(43), 23529–23539.

49 C. Gao, W. Si, Y. Huo, Y. Xiang, G. Li, J. Wang, C. Jia and X. Guo, Device engineering of monolayer-based electronics, *Nano Today*, 2024, **59**, 102472.

50 J. Francis, A. Ramesh and C. S. Sangeeth, Self-assembled monolayer-based electronic devices, *Nanoelectronics Devices: Design, Materials, and Applications (Part I)*, 2023, pp. 33–77.

51 Z. Xie, I. Bâldea and C. D. Frisbie, Why one can expect large rectification in molecular junctions based on alkane monothiols and why rectification is so modest, *Chem. Sci.*, 2018, **9**(19), 4456–4467.

52 S. Y. Quek, M. Kamenetska, M. L. Steigerwald, H. J. Choi, S. G. Louie, M. S. Hybertsen, J. B. Neaton and L. Venkataraman, Mechanically controlled binary conductance switching of a single-molecule junction, *Nat. Nanotechnol.*, 2009, **4**(4), 230–234.

53 Y. Lee, B. Carsten and L. Yu, Understanding the anchoring group effect of molecular diodes on rectification, *Langmuir*, 2009, **25**(3), 1495–1499.

54 M. F. Jamali, H. R. Soleimani and M. B. Tagani, The maximum rectification ratio of pyrene-based molecular devices: a systematic study, *J. Comput. Electron.*, 2019, **18**, 453–464.

55 P. Moreno-García, M. Gulcur, D. Z. Manrique, T. Pope, W. Hong, V. Kaliginedi, C. Huang, A. S. Batsanov, M. R. Bryce, C. Lambert and T. Wandlowski, Single-molecule conductance of functionalized oligoynes: length dependence and junction evolution, *J. Am. Chem. Soc.*, 2013, **135**(33), 12228–12240.

56 S. K. S. Mazinani, R. V. Meidanshahi, J. L. Palma, P. Tarakeshwar, T. Hansen, M. A. Ratner and V. Mujica, Polarizability as a molecular descriptor for conductance in organic molecular circuits, *J. Phys. Chem. C*, 2016, **120**(45), 26054–26060.

57 C. Van Dyck and M. A. Ratner, Molecular junctions: Control of the energy gap achieved by a pinning effect, *J. Phys. Chem. C*, 2017, **121**(5), 3013–3024.

58 A. E. Haj-Yahia, O. Yaffe, T. Bendikov, H. Cohen, Y. Feldman, A. Vilan and D. Cahen, Substituent variation drives metal/monolayer/semiconductor junctions from strongly rectifying to ohmic behavior, *Adv. Mater.*, 2013, **25**(5), 702–706.

59 D. Fracasso, M. I. Muglali, M. Rohwerder, A. Terfort and R. C. Chiechi, Influence of an atom in EGaIn/Ga2O3 tunneling junctions comprising self-assembled monolayers, *J. Phys. Chem. C*, 2013, **117**(21), 11367–11376.

60 W. Du, X. Chen, T. Wang, Q. Lin and C. A. Nijhuis, Tuning overbias plasmon energy and intensity in molecular plasmonic tunneling junctions by atomic polarizability, *J. Am. Chem. Soc.*, 2024, **146**(31), 21642–21650.

61 C. S. S. Sangeeth, A. Wan and C. A. Nijhuis, Equivalent circuits of a self-assembled monolayer-based tunnel junction determined by impedance spectroscopy, *J. Am. Chem. Soc.*, 2014, **136**(31), 11134–11144.

62 H. J. Yoon, C. M. Bowers, M. Baghbanzadeh and G. M. Whitesides, The rate of charge tunneling is insensitive to polar terminal groups in self-assembled monolayers in $Ag^{TS}S(CH_2)_nM(CH_2)_mT//Ga_2O_3$/EGaIn junctions, *J. Am. Chem. Soc.*, 2014, **136**(1), 16–19.

63 X. Chen, H. V. Annadata, B. Kretz, M. Zharnikov, X. Chi, X. Yu, D. A. Egger and C. A. Nijhuis, Interplay of collective electrostatic effects and level alignment dictates the tunneling rates across halogenated aromatic monolayer junctions, *J. Phys. Chem. Lett.*, 2019, **10**(14), 4142–4147.

64 P. Waske, T. Wächter, A. Terfort and M. Zharnikov, Nitro-substituted aromatic thiolate self-assembled monolayers: structural properties and electron transfer upon resonant excitation of the tail group, *J. Phys. Chem. C*, 2014, **118**(45), 26049–26060.

65 H. Wu, Q. Fu, Y. Li, Y. Cui, R. Wang, N. Su, L. Lin, A. Dong, Y. Ning, F. Yang and X. Bao, Controlled growth of uniform two-dimensional ZnO overlayers on Au(111) and surface hydroxylation, *Nano Res.*, 2019, **12**(9), 2348–2354.

66 A. Ulman, Self-assembled monolayers of 4-mercaptobiphenyls, *Acc. Chem. Res.*, 2001, **34**(11), 855–863.

67 X. Chen, H. Hu, J. Trasobares and C. A. Nijhuis, Rectification ratio and tunneling decay coefficient depend on the contact geometry revealed by in situ imaging of the formation of EGaIn junctions, *ACS Appl. Mater. Interfaces*, 2019, **11**(23), 21018–21029.

68 V. Obersteiner, D. A. Egger, G. Heimel and E. Zojer, Impact of collective electrostatic effects on charge transport through molecular monolayers, *J. Phys. Chem. C*, 2014, **118**(38), 22395–22401.

69 E. Zojer, A. Terfort and M. Zharnikov, Concept of embedded dipoles as a versatile tool for surface engineering, *Acc. Chem. Res.*, 2022, **55**(13), 1857–1867.

70 M. Wróbel, T. Żaba, E. Sauter, M. Krawiec, J. Sobczuk, A. Terfort, M. Zharnikov and P. Cyganik, Thermally stable and highly conductive SAMs on Ag substrate—the impact of the anchoring group, *Adv. Electron. Mater.*, 2021, **7**(2), 2000947.

 This journal is © The Royal Society of Chemistry 2025